PREDICTION OF PERFORMANCE IN ITER-FEAT

HIROSHI MATSUMOTO* and PIETRO BARABASCHI
ITER Joint Central Team, Garching Joint Work Site, D-85748 Garching, Germany

YOSHIKI MURAKAMI *ITER Joint Central Team*
Naka Joint Work Site, Naka, Ibaraki-ken, 311-01 Japan

Recently, the technical objectives of ITER were redefined aiming at a cost reduction of ~50% from the 1998 ITER design. Machine parameters that would satisfy the revised technical requirements under the engineering constraints were specified using a system code. The performances of the 1998 ITER and a redefined machine were studied and compared. As a result of these studies, final machine parameters were determined with revised conservative physics assumptions. This redefined machine is referred to as ITER-FEAT. It was shown that ITER-FEAT would achieve $Q = 10$ in inductive operation with reasonable and conservative assumptions. Also, with an efficient current drive system and modest confinement improvement, the possibility of $Q = 5$ noninductive operations in a steady state was shown.

I. INTRODUCTION

The options of the Reduced Technical Objectives/Reduced Cost (RTO/RC) ITER aimed at a target of ~50% of the cost of the 1998 ITER design[1] while maintaining its overall programmatic objective have been studied. The newly set requirements of the reduced objectives[2] are as follows:

The device should

1. achieve extended burn in inductively driven plasmas with a ratio of fusion power to auxiliary heating power of at least 10 for a range of operating scenarios and with duration sufficient to achieve stationary conditions on the timescales characteristic of plasma processes. In addition,

the possibility of controlled ignition should not be precluded

2. aim at demonstrating steady-state operation using noninductive current drive (CD) with the ratio of fusion power to input power for a CD of at least 5

3. demonstrate the availability and integration of technologies essential for a fusion reactor [such as superconducting (SC) magnets and remote maintenance]

4. test components for a reactor (such as systems to exhaust power and particles from the plasma)

5. test tritium-breeding module concepts that would lead in a future reactor to tritium self-sufficiency, the extraction of high-grade heat, and electricity generation.

In this paper, the process of selecting the main parameter sets under these requirements are described first. Then, two representative options selected for rigorous exploration and quantification of the issues and costing are described, i.e., the intermediate aspect ratio machine (IAM) with a high toroidal magnetic field, single-null (SN)-divertor vertically asymmetric magnetic configuration, and the low aspect ratio machine (LAM) with a low toroidal field, lower aspect ratio, and vertically symmetric design able to support (if proved useful) a double-null (DN) divertor. The IAM and LAM plasma performance predicted by the PRETOR 1.5-dimensional transport code[3] is presented. Finally, after careful study of the RTO/RC ITER designs the parameters and predicted performance of the ITER-FEAT machine is described.

II. PHYSICS ASSUMPTIONS

The physics assumptions are basically the same as those used in 1998 ITER (Ref. 1). The high confinement

*E-mail: matsumh@itereu.de

mode with the edge-localized mode instability (ELMy H-mode) is chosen as the reference operation regime. The ELMy H-mode is well studied in the present experiments, and a large database is available for projection of essential parameters to ITER.

The key quantities that determine the plasma performance are

1. the thermal energy confinement time τ_E

2. the impurity level in the main plasma

3. the normalized plasma density n_e/n_{GW} with $n_{GW} = I_p/(\pi a^2)$

4. normalized plasma pressure $\beta_N = \beta(aB_o/I_p)$

5. normalized power crossing the plasma separatrix P_{loss}/P_{LH}, where P_{LH} is the H-mode power threshold given by

$$P_{LH} = 0.9 \times BR^2 n^{0.75}/M \text{ (MW)}$$

where n is in 10^{20} m^{-3}.

The fusion performance is expressed as a domain indicating how key figures of merit (FOMs) such as the fusion power P_{fus} or the power multiplication factor $Q = P_{fus}/P_{aux}$ (P_{aux} is externally applied plasma heating power) vary within the plausible range of input parameters. The IPB98(y,1) ELMy H-mode confinement scaling law[4]

$$\tau_{E,th}^{IPB98(y,1)}(s) = 0.0503 H_{H98y1} I_{MA}^{0.91} B_T^{0.15} P_{MW}^{-0.65} n_{19}^{0.44}$$
$$\times M^{0.13} R_m^{2.05} \epsilon^{0.57} \kappa_a^{0.72}$$

is used for normalization of heat transport coefficients. The impurity level is determined with the same divertor model as previously used for the 1998 ITER (Ref. 1) after renormalization to take into account the new geometry of the divertor, updated pumping speed, and target plate geometry. Extrapolations from present-day experiments show that the ELMy H-mode can provide adequate confinement and allow sustained stationary plasma operation with low impurity concentration, controlled density, high plasma beta, and adequate helium transport to the plasma boundary.

III. SYSTEM ANALYSIS

To find a set of consistent overall parameters of a tokamak device, one needs to solve a set of nonlinear equations that describe different aspects of the machine performance, both in engineering and in physics. These equations often represent simplifications of much more complex phenomena and can be combined with a root-finding algorithm to form what we often call a system code.

In this system approach, the equations that define the physics performance and power balance are often zero-dimensional including the customary scaling law for energy confinement predictions. Plasma temperature can be calculated based on power balance expressions.

Plasma density is limited by the density limit itself or by the β_N limit.

Engineering equations, both for plasma and structures, can be more detailed but, with some generally applicable exceptions, must be extracted and qualified by a specific design solution already studied in detail.

A costing algorithm usually completes the suite of procedures that constitute a system code by giving the capability to investigate cost trends as a function of dependent variables. This section of the system code typically constitutes its greatest limit in that costing is performed with continuous functions that can only grossly approximate the real costs.

Together with all types of equations and algorithms, one needs to consider boundary conditions, limits, and parameters. These, for example, include conditions on Q, limits on β_N, plasma density, the edge safety factor, material allowable stresses, etc.

To better clarify the process included in the system code analysis, the flow diagram shown in Fig. 1 indicates in simple terms the procedure by which global sizing of a tokamak can be found:

1. Some conditions are specified. These include the power amplification factor Q, magnetohydrodynamic (MHD) safety factor, burn flux capability, peak field in toroidal field (TF) and central solenoid (CS) magnets, space allocated for shielding, confinement enhancement factor H_H (Ref. 4), operating point normalized beta β_N, plasma elongation, and normalized density n/n_{GW}.

2. Tentative initial values for the major (R) and minor (a) radii are established.

3. Cross-sectional sizes as well as global dimensions, shape, number of coils, and current for the TF magnet are found.

4. The peak possible plasma current is now evaluated.

5. The burn flux is then calculated and compared with the specification. The minor radius is consequently adjusted, and the code loops back to point 3 up to when the burn duration is as required.

6. The plasma parameters are then computed with a zero-dimensional procedure. The beryllium fraction is assumed fixed. The helium fraction is computed based on fusion power and confinement. The density is determined by the specified value of β_N and/or by the density limit. The energy confinement time is adjusted to take into account the L-H transition power scaling. The plasma temperature is self-consistently calculated to satisfy the power balance in the plasma.

7. Finally, the value of Q is computed and compared with the specification. The major radius is consequently adjusted, and, if required, the program loops back to point 3 until Q reaches the desired value (in our case ~ 10).
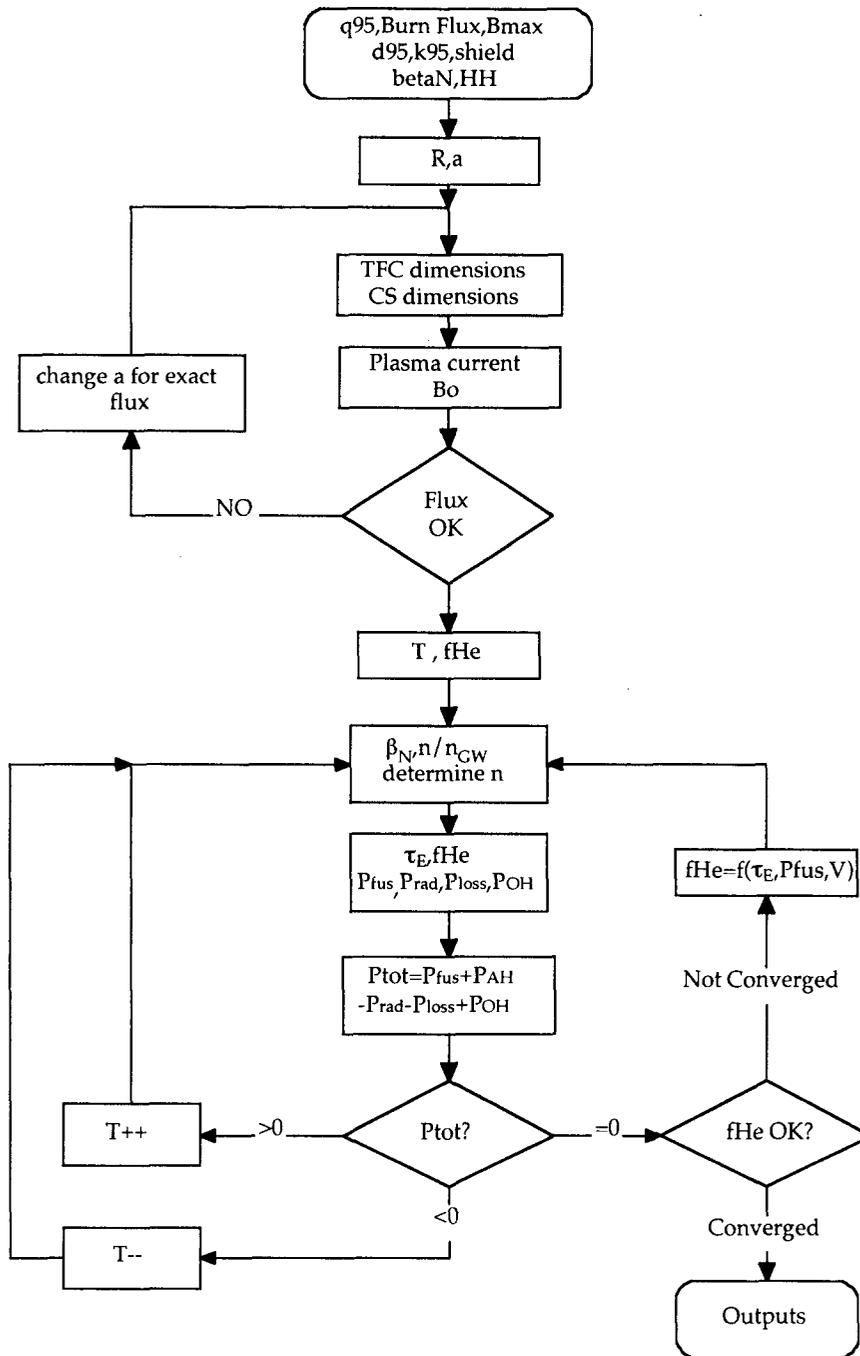
q95,Burn Flux,Bmax
d95,k95,shield
betaN,HH

R,a

TFC dimensions
CS dimensions

change a for exact flux

Plasma current
Bo

Flux OK

NO

T , fHe

β_N,n/n_{GW} determine n

τ_E,fHe
Pfus,Prad,Ploss,POH

fHe=f(τ_E,Pfus,V)

Ptot=Pfus+PAH
-Prad-Ploss+POH

Not Converged

T++

>0

Ptot?

=0

fHe OK?

<0

T--

Converged

Outputs

Fig. 1. Flowchart for system code.

It is important to point out that for any given finite Q, four parameters, i.e., the aspect ratio, maximum toroidal field, elongation, and poloidal magnetic flux consumed during the plasma burn phase (burn flux) are not mutually independent. Allowable elongation, with a given set of vertical position and shape control constraints, is in fact also a function of the aspect ratio. Moreover, for any given burn flux and aspect ratio, the peak field in the TF magnet is automatically determined unless some space is wasted. It is also important to mention that the limit on plasma triangularity is strongly interconnected with the divertor geometry, shape control, and issues related to the SN divertor operation, such as distance between active and inactive separatrixes. For the divertor operation, this is characterized as a physical distance rather than a flux separation.

The main design inputs and outputs of the system code are summarized in Table I.

TABLE I

The Main Design Inputs and Outputs of the System Code

Inputs	Outputs
Aspect ratio (or peak toroidal field)	Dimensions of structures
Beta limit, β_N	Fusion power, P_{fus}
Burn flux	Helium fraction, n_{He}/n_e
Confinement enhancement, H_H	Machine cost
Density limit, n/n_{GW}	Major radius, R
Elongation at 95% flux	Minor radius, a
[or $\kappa_{95} = f(A)$]	
Helium criteria, e.g., τ_{He}/τ_E	Plasma current, I_p
Peak CS field	Plasma density, $\langle n_e \rangle$
Power amplification factor, Q	Plasma temperature, $\langle T_e \rangle$
Safety factor at 95% flux surface,	Toroidal field at R, B_o
q_{95}	
Shielding and clearance	
requirements	
Structural and SC criteria	
Triangularity, δ (or inner divertor	
length)	

III.A. Sensitivity to Aspect Ratio

An analysis has been performed, under the constraints explained earlier, by varying the required aspect ratio. The burn flux has been assumed fixed and equal to the value of 30 Wb.

In this specific study, the elongation measured at the 95% flux surface was changed as a function of the aspect ratio following the linear relation shown in Fig. 2 to take into account the higher plasma natural elongation as well as the more favorable ratio between the minor radius and blanket shielding thickness at a lower aspect ratio.

As shown in Fig. 3, the following tendencies are observed as the aspect ratio is increased:

1. The major radius reduces somewhat, while the minor radius reduces more significantly.

2. Both the TF magnet peak value and the toroidal magnetic field at the plasma center increase.

3. The plasma current decreases together with plasma volume and wall area.

4. Both density and density normalized to the Greenwald density increase.

5. The magnetic energy and the TF magnet weight increase while the first-wall area together with the blanket/vacuum vessel weights decreases. This practically means that costs associated with the magnet system increase while the ones associated with the vacuum vessel/blanket decrease.

6. The estimated cost has a rather weak variation with a minimum somewhere between an aspect ratio of 2.8 and 3.5. The actual value of the aspect ratio A, where this minimum occurs easily, changes within this range on the basis of small modifications of the costing or engineering assumptions.

It is therefore clear that no particular decision can be made on the optimal aspect ratio based on cost alone.

III.B. Plasma Elongation and Triangularity

The IPB98(y,1) ELMy H-mode confinement scaling law contains the dependence on the plasma elongation κ. The confinement improves with the increase of κ. However, experimental data that support the validity of the scaling beyond $\kappa_x = 1.9$ are very scarce. Also, control of plasma vertical stability becomes very difficult at high κ. Then, the maximum elongation should be $\kappa_x = 1.9$.

A higher triangularity allows an increase of the plasma density and beta with good plasma confinement. However, the amount of energy expelled per edge-localized mode (ELM) increases with an increase of triangularity. This can reduce the lifetime of the divertor plate.
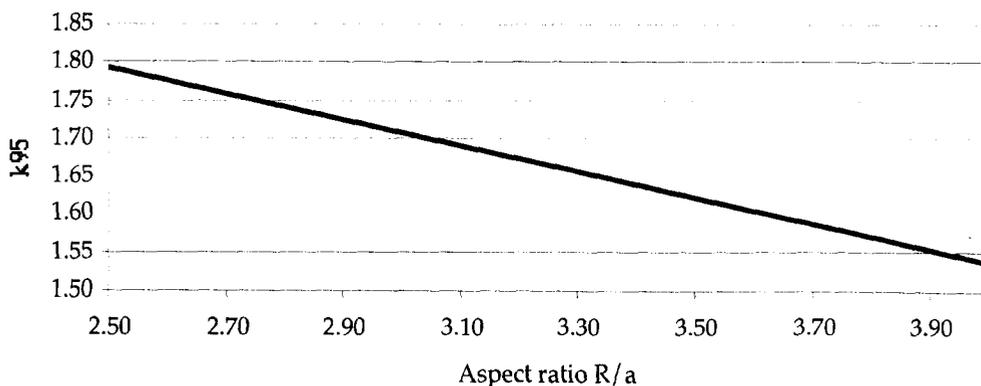

Fig. 2. Dependence of k_{95} versus plasma aspect ratio used in the system code for aspect ratio scans.
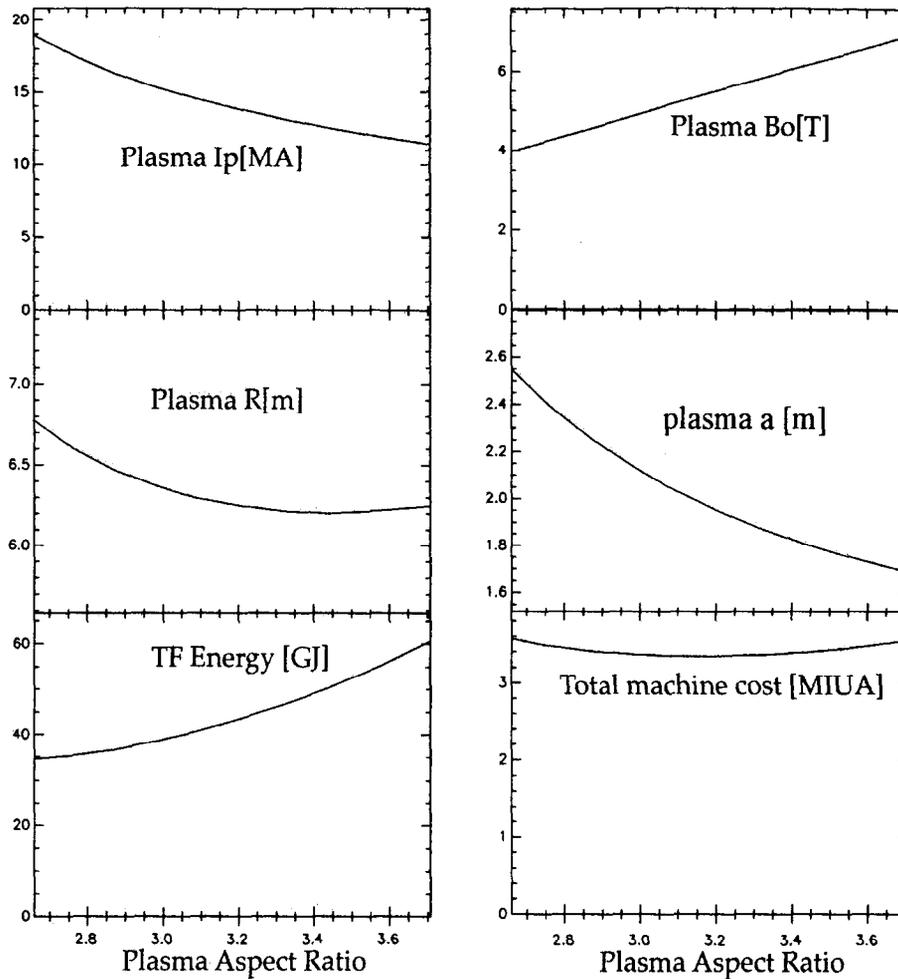
Fig. 3. Variation of some tokamak parameters as a function of aspect ratio.

Therefore, a moderately high triangularity ($\delta_{95} \sim 0.35$) was chosen.

To resolve the choice and better appreciate the effects of plasma volume versus the strength of the toroidal field at constant Q, or in other words the effect of changing A, machine layouts at $A = 2.8$, 3.3, and 3.5 were carefully examined and compared. However, it is clear from the study that an ITER scale device with high aspect ratio such as $A = 3.5$ has a serious difficulty in accessibility and increases cost because of a larger outboard radius of the TF coils (TFCs). As a consequence, two distinct example layouts and specific sets of parameters are presented for further detailed study:

1. IAM: with an aspect ratio of ~3.3, SN divertor, asymmetric magnetic configuration

2. LAM: with an aspect ratio of ~2.8, symmetric configuration and ability to support (if proven useful) a DN divertor owing to a larger available space in the vacuum vessel than IAM.

The main parameters of these machines are shown in Table II.

These examples of RTO/RC ITER are used in Sec. IV to evaluate in detail their performances, to analyze specific engineering solutions, to identify their margins, and to quantify their costs.

IV. RTO/RC ITER PLASMA PERFORMANCE

The modeling of the plasma performance in IAM and LAM was performed using the PRETOR 1.5-dimensional transport simulation code.

IV.A. Inductive Operation

This section concentrates on inductive ELMy H-mode deuterium-tritium (D-T) operation with a prescribed plasma current satisfying $q_{95} = 3$.

TABLE II

The Main Parameters of IAM and LAM

Parameters	IAM	LAM	Parameters	IAM	LAM
R (m)	6.20	6.45	Plasma volume (m³)	726	1177
a (m)	1.90	2.33	Elongation, κ_{95}	1.68	1.74
I_p (MA)	13.3	17	Elongation (effective), κ_a	1.83	1.92
B_o (T)	5.51	4.23	Average triangularity, δ_a	0.43	0.49
Aspect ratio	3.26	2.77	Number of coils	18	20
q_{95}	3.00	3.00	Total TF current (MA)	171	136
Peak toroidal field (T)	12.4	10	TF energy (GJ)	44	32
Plasma external surface (m²)	632	824	1 TFC tension (MN)	120	70
Plasma section surface (m²)	19.40	30.12	1 TFC radial force in inboard (MN)	59	35

IV.A.1. Reference Parameters

Under the foregoing modeling assumptions, the kinetic profiles predicted for IAM and LAM under $Q = 10$ reference conditions are shown in Figs. 4a and 4b. The global parameters for these reference discharges are given in Table III.

IV.A.2. Operational Domains

The operational domain is a tool used to determine the main plasma parameters, such as density, normalized toroidal beta, or loss power normalized to the power required to sustain the H-mode as a function of confinement as expressed by the H_H factor. In computing the
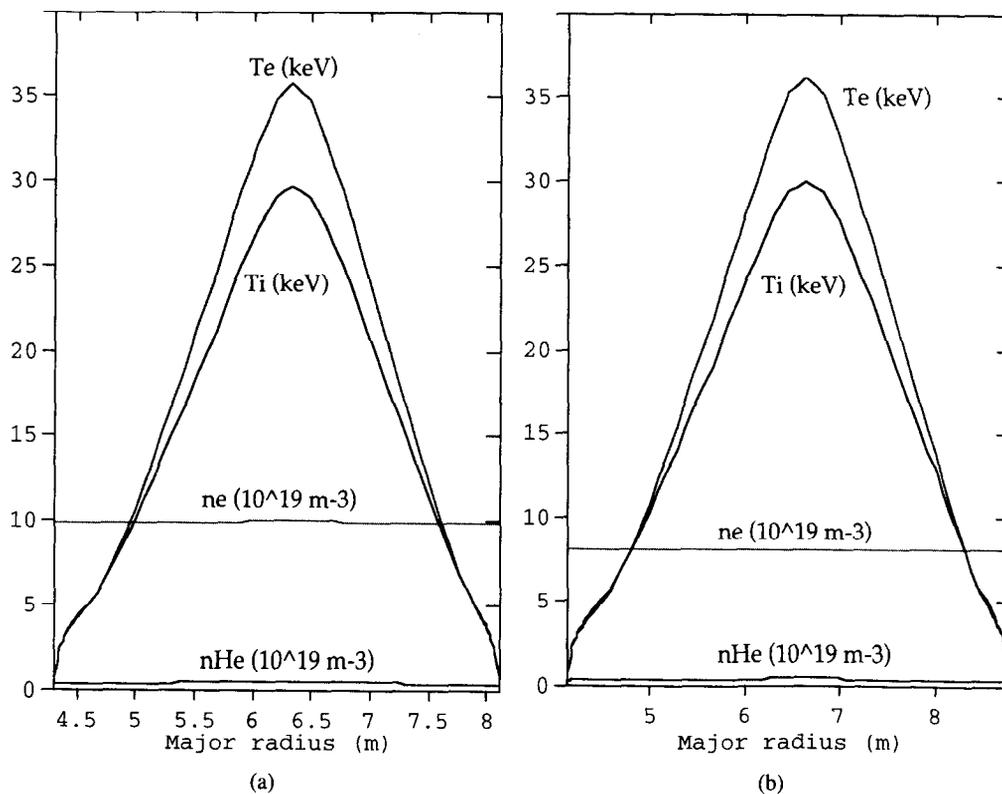

Fig. 4. Temperature and density profiles of (a) IAM and (b) LAM.

TABLE III

Main Plasma Parameters of IAM and LAM at Inductive $Q = 10$ Operation

Parameter	IAM	LAM	Parameter	IAM	LAM
n_e (10^{19} m^{-3})	10	8	τ_{He}/τ_E	5	5
$\langle T \rangle$ (keV)	11	11	n_e/n_{GW}	0.8	0.8
Z_{eff}	1.9	2.0	H_H	1.0	1.0
P_{aux} (MW)	50	50	β_N	2.1	2.2
P_{fus} (MW)	500	500	P_{fus}/S_{surf} (MW/m^2)	0.8	0.6
τ_E (s)	3.2	4.2	Loop voltage (mV)	70	80

operation domain, a zero-dimensional transport model was used with plasma profiles calibrated by the 1.5-dimensional transport code. By indicating on the same diagram the location of limits, i.e., the density, beta, and H-mode power threshold, one can determine which range of confinement is acceptable while achieving a given Q and obeying operational limits.

IV.A.3. $Q = 10$ domains

Figures 5a and 5b indicate the domain for $Q = 10$ for IAM and LAM, respectively. Each point of the domain corresponds to $Q = 10$. The shaded area indicates the region—in terms of range of fusion power and H_H factor—that obeys the following limits: $n/n_{GW} < 1$,
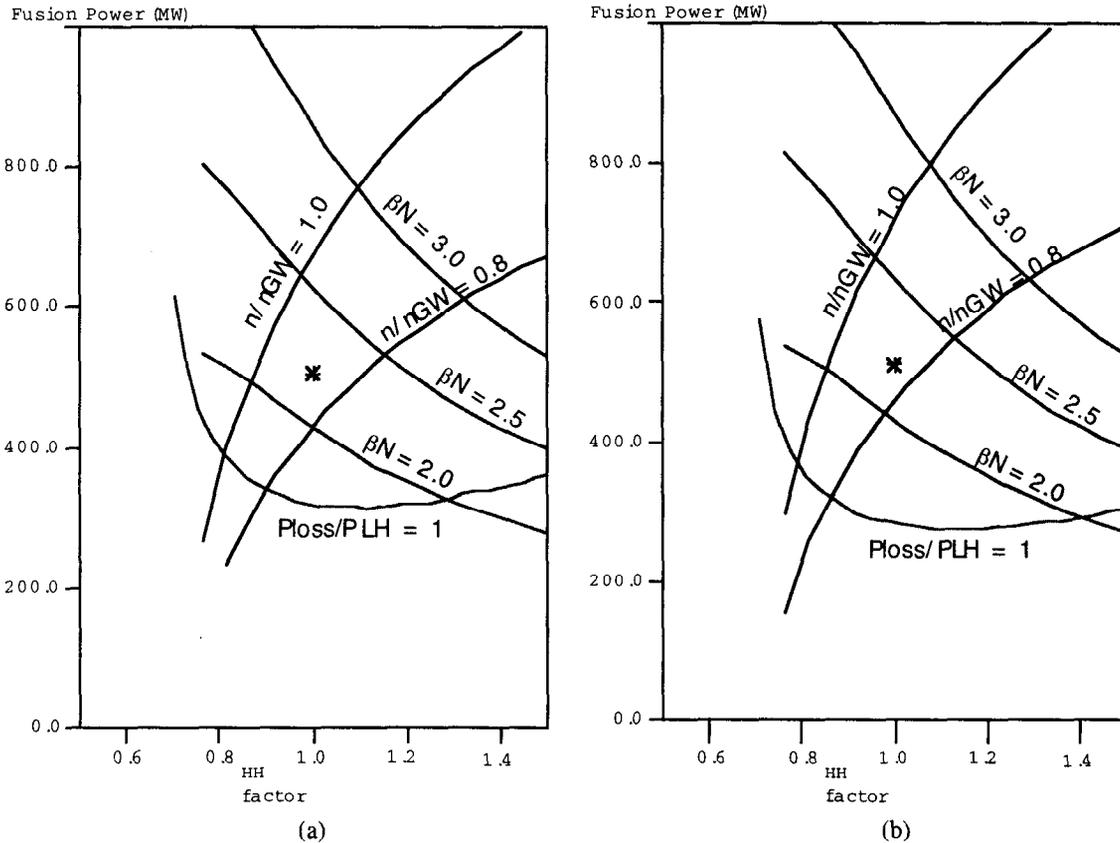

Fig. 5. The $Q = 10$ operation domain of (a) IAM and (b) LAM.

$P_{loss}/P_{LH} > 1$, and $\beta_N < 2.5$. It is observed in all major divertor tokamaks that the energy confinement starts to drop near the Greenwald density. Also, in monotonic q profile discharges, it is generally observed that the confinement begins to degrade near $\beta_N = 2.5$ although the ideal MHD limit is higher. To keep the discharge in H-mode, $P_{loss}/P_{LH} > 1$ is needed. Adequacy and range of validity in these limits are explained in Ref. 4. The domain indicates that the fusion power is limited at the upper end by the beta limit and at the lower end by the L-H power threshold. In absolute terms, these fusion power limits are similar between the design variants. As confinement is reduced, maintaining the fusion power requires an increase in the plasma density.

IV.A.4. Ignited Domains

Ignition is not precluded in any device but would require operating closer to the conservative limits mentioned earlier. In particular, since the loss power is reduced compared to the $Q = 10$ case, the line $P_{loss}/P_{LH} = 1$ moves to higher values of fusion power. Reaching ignition therefore requires operation at high power (>600 MW), high density ($n/n_{GW} \sim 1$), β_N values above ~2.5, and good confinement ($H_H > 1$). These stringent operational requirements can be relaxed significantly by operating at higher plasma current with q_{95} below 3, which allows potentially better confinement and higher Greenwald density. The ignited domain for IAM is sufficiently secured with $q_{95} = 2.6$, as seen in Fig. 6. Similar effects (higher Greenwald density and potentially better confinement) can be obtained with an increased plasma elongation.

IV.B. Noninductive Operation

Prediction of plasma performance in noninductive steady-state operation has inherent difficulties arising from the following facts. The total driven plasma current depends on profiles of plasma parameters that are interrelated. Confidence in the prediction of the density profile and plasma purity is rather low because of the density peaking often observed in these regimes, which could decouple the edge density from the volume-averaged density. The control of the current density profile, which should satisfy equilibrium and stability criteria, is not easy, and optimization of noninductive operation in terms of the fusion output Q is not trivial.

IV.B.1. Monotonic q Profile Scenario

The simplest scenario of noninductive operation would be a monotonic q operation by injecting momentum and energy at the center of the plasma. Almost the best CD efficiency can be obtained at the hottest core of the plasma, and also, the power is coupled to the most efficient spot for fusion reactions. However, excessive current density at the center of the plasma would create
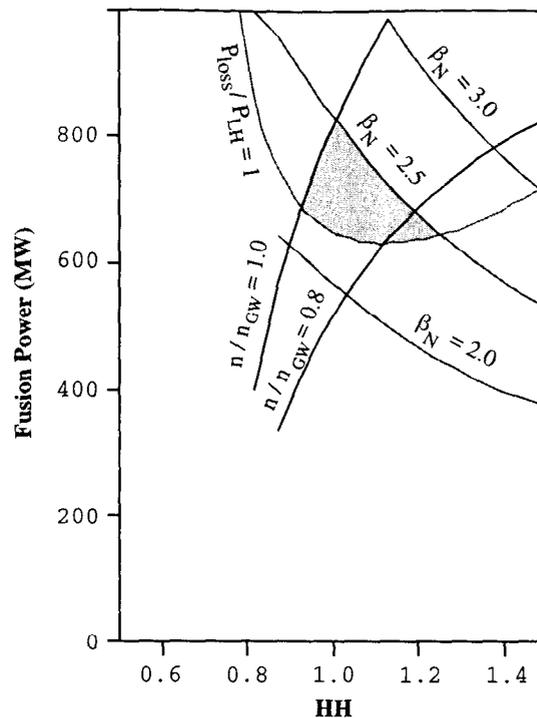

Fig. 6. Ignited domain for IAM at $q_{95} = 2.6$.

strong and frequent sawtooth oscillations, and the contribution of bootstrap current is rather small because of the more centrally peaked pressure profile. In this section, a steady-state scenario for IAM with a centrally driven current and modest confinement improvement is considered. In the simulation with PRETOR, a generalized CD module was used. With this module, instead of computing CD efficiency of each CD scheme, CD efficiencies γ^* and profiles were given to the code as input. Here, γ^* is the CD efficiency normalized at the electron temperature of 10 keV: $\gamma^* = \gamma (10 \text{ keV}/T_e)$, where γ is the usual FOM for CD efficiency in 10^{20} MA/MW·m^{-2}.

Note the following assumptions and input to the simulations:

1. 80 MW of the CD power (50% coupling of the CD power to electrons and 50% to ions)

2. width of the CD power deposition profile: 25% in minor radius around the plasma center

3. CD efficiency: $\gamma^* = 0.20$.

4. $H_H = 1.1$.

The results of the simulation are as follows:

1. thermal $Q = 4.8$

2. normalized beta, $\beta_N = 2.5$, beta poloidal = 1.4
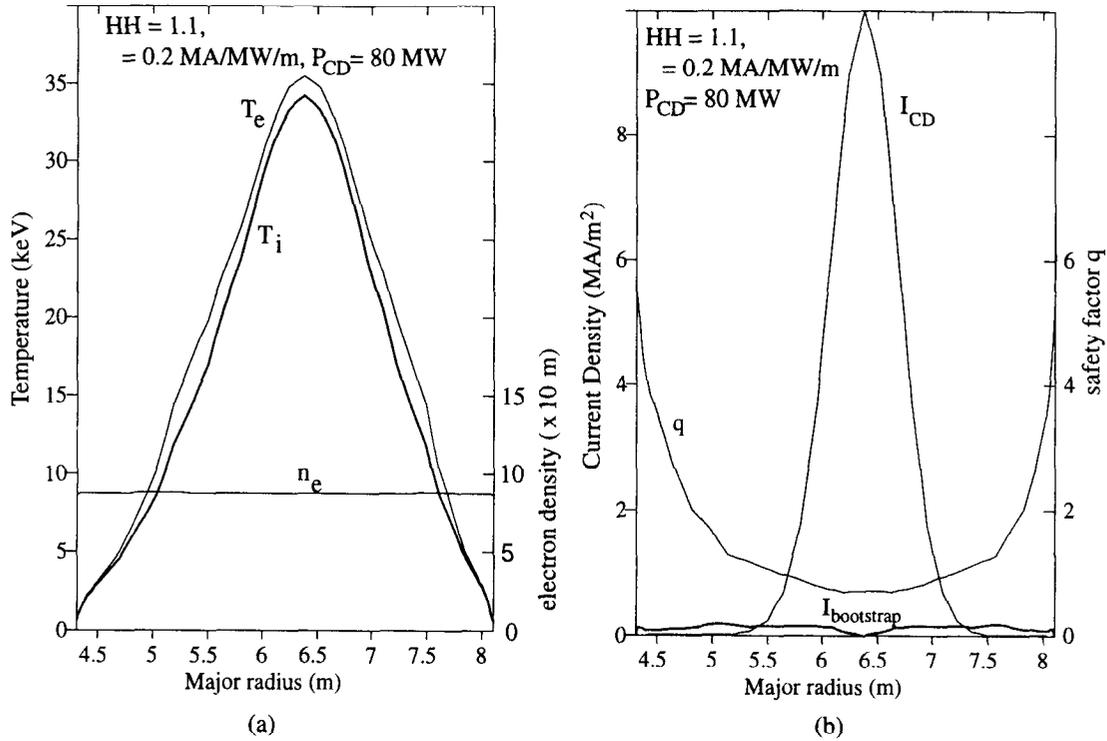
3. volume-averaged quantities

Fig. 7. (a) Temperature and density profiles and (b) current profiles and q profile of the noninductive operation simulated by 1.5-dimensional transport code.

a. $T_e = 10.7$ keV, $T_i = 9.5$ keV, $n_e = 8.8 \times 10^{19}$ m^{-3}, $Z_{eff} = 1.7$

b. I_p (total) $= 10.3$ MA ($I_{bootstrap} = 2.4$ MA, $I_{CD} = 7.9$ MA), $q_{95} = 4.4$, $l_i = 1.1$.

Figure 7a shows the electron and ion temperature profiles and density profile. Figure 7b shows the safety factor q profile and the driven current density profiles.

Dependence of Q on the confinement improvement factor H_H with the CD efficiency γ as a varying parameter is shown in Figs. 8 and 9. Figure 8 shows the case with 100 MW of the CD power input. When the CD power of 100 MW is available, either very high CD efficiency, $\gamma^* = 0.25$ and $H_H = 1$, or a conservative CD efficiency of $\gamma^* = 0.15$ and moderate confinement improvement $H_H = 1.2$ will be needed to reach the $Q = 5$ region. However, the operation region of high confinement and low CD efficiency tend to give higher normalized beta compared with the operation region of modest confinement and high CD efficiency for the same Q value. Figure 9 shows the achievable Q for CD powers of 60, 80, and 100 MW with the fixed CD efficiency of $\gamma^* = 0.20$. With this CD efficiency, $H_H = 1.15$ is needed when the CD power is 80 MW to reach $Q = 5$. If the available heating power is not more than 60 MW, a significant improvement of confinement, $H_H > 1.4$, will be needed to achieve $Q = 5$.
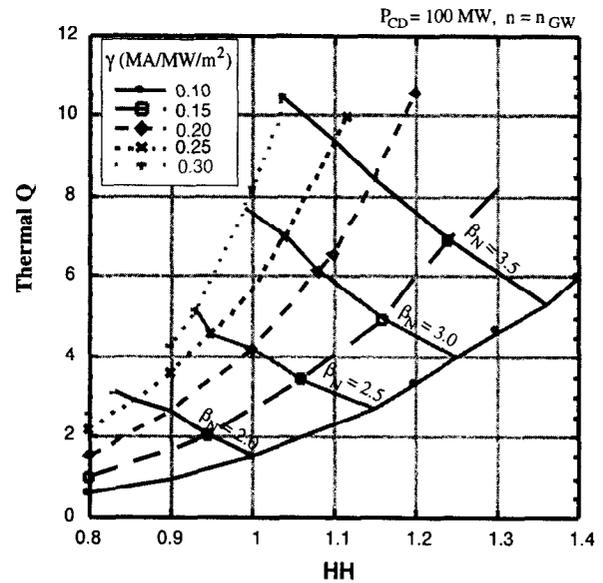

Fig. 8. Effect of CD efficiency on the $Q = 5$ operation domain.

IV.C. Reversed Shear Configuration

Recently, a substantial increase of confinement is observed in large tokamaks with reversed magnetic shear
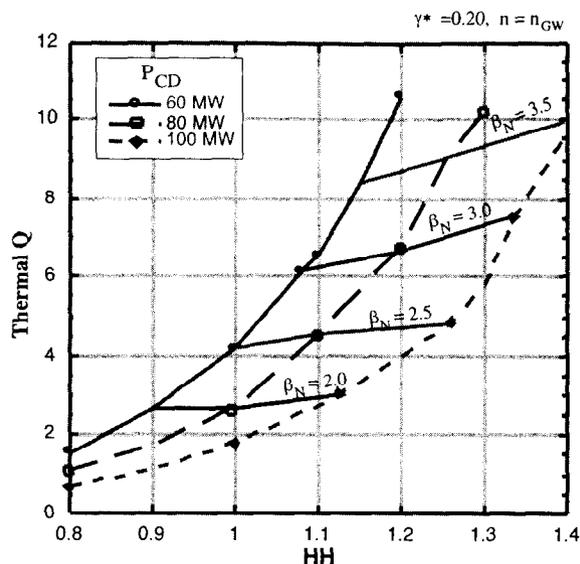
$\gamma^* = 0.20, n = n_{GW}$

Fig. 9. Effect of CD power on the $Q = 5$ operation domain.

20 MW NBI(1000kV) at the center
60 MW RF ($\gamma^* = 0.2$) off axis for creation of ITB

Fig. 10. Radial position of the ITB and improvement of confinement.

configurations.[5-8] The internal transport barrier (ITB) appears inside the plasma around the location of q minimum in this magnetic configuration. Although the theoretical and experimental bases are not firm enough, this is certainly an attractive operation regime for the steady-state operation of ITER. For the purpose of the simulation, this confinement improvement regime is characterized by the radial location of the ITB and the percentage of the uniform reduction in transport within this barrier. In this simulation, the ITB was set up by the intense localized CD, 60 MW, with a CD efficiency of $\gamma^* = 0.2$; 20 MW of neutral beam injection (NBI) heating at 1000 kV was applied with a beam tangency radius of 5.2 m on the plasma midplane. Improvement of the confinement in terms of the H_H factor was plotted against the radial position of the ITB with the amount of transport reduction as a varying parameter. The results are shown in Fig. 10. Figure 10 suggests that both a strong barrier and wide region of improved confinement are simultaneously required to achieve overall significant confinement improvement.

However, the wider the region of improved confinement is established, the lower the internal inductance l_i becomes. The ideal MHD external kink mode becomes a considerable threat owing to the high current densities near the wall. Without a conducting wall, an ideal limiting β_N of 2.5 is predicted.[4] The wall would be capable of providing the needed stability were it not for the resistive wall mode.[9] Also, recent detailed study shows that the limit on obtainable beta is better described by[10] $\beta_{N,max} \sim 4\, l_i$ where l_i is the plasma internal inductance. And, stabilization of this mode seems increasingly difficult with a very wide region of the confinement improvement, which can be characterized by an extremely small l_i. Also, if the CD power is mostly spent in the edge, the
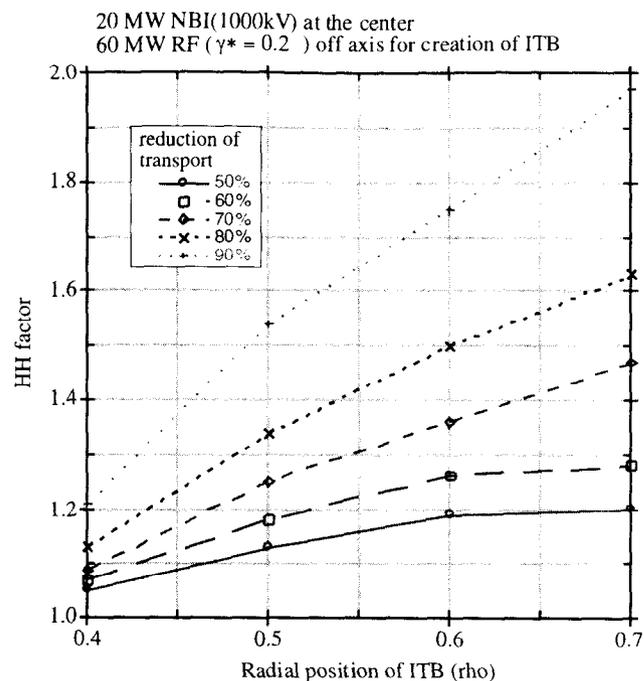
overall efficiency for fusion power production is not necessarily very good.

Figure 11 shows the thermal Q of these discharge points. The numbers shown near the plotting points are the ratio of the normalized beta to the internal inductance. It is clear that the operation points with both a wide region of improvement and a strong barrier have ratios much higher than 4.

Typical parameters for the IAM and LAM devices under $Q = 5$ steady-state reverse magnetic shear operation are shown in Table IV.

In a series of simulations, Q under noninductive operation has been calculated while varying the H_H factor, the CD efficiency γ^*, and the CD power. The simulations indicate that Q is most sensitive to H_H and the product of the CD efficiency and power $(\gamma^* \times P_{CD})$. Figure 12 plots β_N as a function of $(\gamma^* \times P_{CD})$ for three values of the H_H factor: 1, 1.25, and 1.5. For $Q = 5$, the required values of β_N decrease significantly with the $(\gamma^* \times P_{CD})$ product. At the low end of $(\gamma^* \times P_{CD})$ (<15), high β_N's = 3.5 to 4 are required. This, combined with a requirement of significant confinement improvement, will need an advanced tokamak mode of operation. At higher values of $(\gamma \times P_{CD})$ (>20), the required β_N's are smaller (3 to 3.5), and only modest confinement improvement is required. Figure 12 also indicates that the required values of β_N are systematically $\sim 10\%$ lower for IAM than for LAM at fixed Q. This systematic difference has to be attributed to the

20 MW NBI(1000kV) at the center
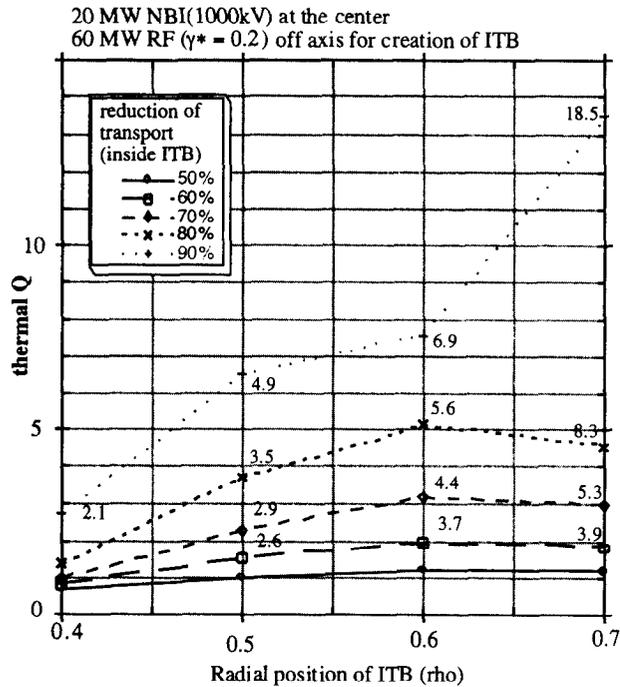60 MW RF (γ* = 0.2) off axis for creation of ITB

Fig. 11. Radial position of ITB and achievable thermal Q value.

higher aspect ratio leading to lower plasma current and higher bootstrap current fraction.

V. COMPARISON BETWEEN IAM AND LAM

Comparative studies on two options of the RTO/RC ITER, IAM and LAM, have been carried out, and the following conclusions were obtained based on IPB98(y,1) ELMy H-mode confinement scaling law:

1. The IAM and LAM options of the RTO/RC ITER can achieve $Q = 10$ in inductive operation at $H_H = 1$ with conservative values of operating density ($\cong 0.85n_{GR}$),

normalized beta ($\beta_N \cong 2.2$), and $P_{loss}/P_{LH} > 1.4$. LAM has a higher margin in P_{loss}/P_{LH}.

2. Values of Q achievable at steady-state noninductive operation are sensitive to the CD efficiency and CD power and to the level of the confinement improvement over the ELMy H-mode scaling prediction and β_N.

3. With an efficient CD system and power of ~100 MW, only a modest confinement improvement ($H_H > 1$ to 1.2) would be required to achieve $Q = 5$ in either IAM or LAM at steady-state operation.

4. IAM has a higher Greenwald density and is favorable for divertor operation.

5. Because of its higher aspect ratio, IAM needs smaller (by 10 to 20%) values of H_H and β_N to achieve $Q = 5$ compared to LAM.

VI. ITER-FEAT

A lower aspect ratio device has a lower toroidal magnetic field, a higher plasma current, a larger minor radius, and more margins in L-H transition power than a higher aspect ratio device. A higher aspect ratio device provides a higher fusion power density and a more favorable capability for steady-state operation. It requires a smaller confinement improvement and a smaller normalized beta than a lower aspect ratio device to achieve $Q = 5$ in steady-state operation. A higher aspect ratio gives a higher Greenwald density and is favorable for divertor operation. However, it became apparent that a high aspect ratio device such as 3.5 in the level of the RTO/RC ITER devices has a serious difficulty in accessibility and increases cost because of a larger outboard radius of the toroidal coils.

The best compromise for achieving the required inductive and noninductive plasma performances and for operating at a high enough plasma density to satisfy divertor target power flux limits while keeping the density

TABLE IV

Typical Parameters for IAM and LAM Devices Under Steady-State Reversed Magnetic Shear Operation

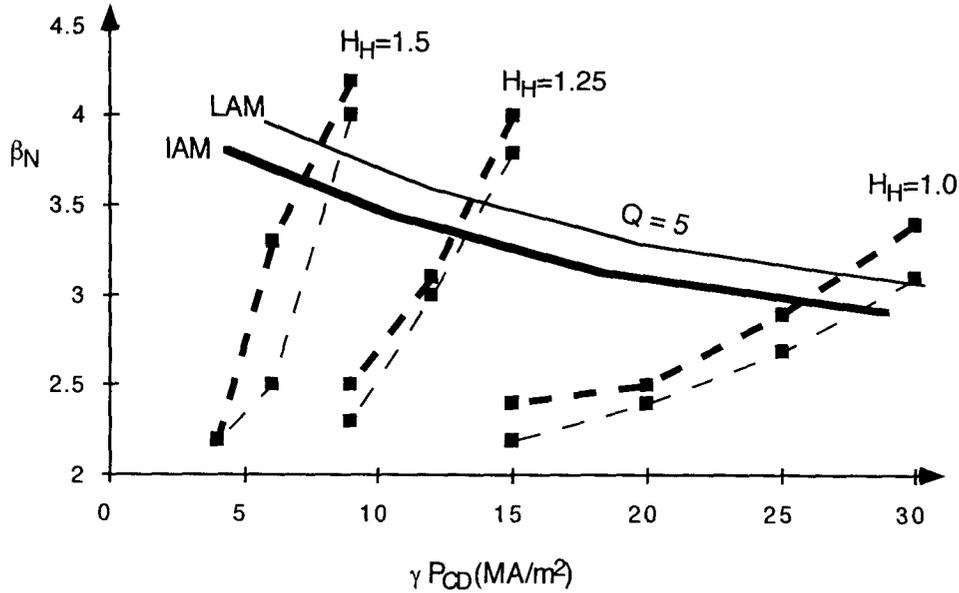| Parameter	IAM	LAM	Parameter	IAM	LAM
R (m)	6.37	6.62	n/n_{GW}	1.0	1.0
a (m)	1.73	2.16	β_N	3.4	3.6
B_T (T)	5.38	4.14	P_{loss}/P_{LH}	2.3	2.9
κ_a	1.93	1.93	$\langle n_{e19} \rangle$	9.9	7.8
I_p (MA)	9.1	11.1	$\langle T \rangle$ (keV)	11.3	10.9
q_{95}	4.4	4.1	β_p	1.98	1.63
f_{bs}	0.44	0.40	P_{fus} (MW)	500	500
H_H	1.25	1.25	P_{CD} (on/off axis) (MW)	20/80	20/80

Fig. 12. Required β_N values as a function of CD FOM ($\gamma \times P_{CD}$). The dotted lines indicate the constant H_H factor contours, and the solid lines indicate the constant $Q = 5$ contours. IAM is indicated by thick lines, and LAM is indicated by thin lines. Two percent of carbon impurity is assumed.

below the Greenwald density would be the IAM model configuration.

Following careful study of these RTO/RC ITERs, a single configuration, referred to as ITER-FEAT, was established. In selecting the machine parameters of ITER-FEAT, two key physics rules were updated following recommendations by the ITER Physics expert group based on recent experimental results.

One of the essential physics rules that enters into the prediction of plasma performance in ITER-FEAT is the scaling of the H-mode threshold power. The newly recommended form for the former scaling is

$$P_{LH} = 2.84 M^{-1} B_T^{0.82} \bar{n}_e^{0.58} R^{1.00} a^{0.81}$$

(in MW, AMU, T, 10^{20} m^{-3}, and m)

[root-mean-square (rms) error 0.268] ,

with M the effective isotopic mass of the plasma fuel. This scaling expression is based on the latest version of the threshold database (DB3) extended with results from recent, dedicated, H-mode threshold experiments in Alcator C-Mod and in JT-60U. For RTO/RC ITER devices, this new scaling yields almost a half of the threshold power as that predicted by an earlier version IPB98(5) with a 95% (i.e., 2σ) confidence interval of $P_{LH}(1.7,0.6)$. There is, however, evidence from the Joint European Torus (JET) and JT-60U that the heating power should be 1.3 to 1.5 times higher than the H-mode threshold to obtain a good H-mode confinement. Therefore, a new rule, $P_{loss} > 1.3P_{LH}$, was adopted.

Another physics rule updated is the scaling of the global energy confinement time. In the ITER Physics Basis (IPB) report,[4] five empirical log-linear (power law) scaling expressions for the energy confinement time are presented that are derived from different subsets of the H-mode global confinement database containing data from 13 tokamak devices. The expressions fall into two distinct groups, of which two expressions, IPB98(y) and IPB98(y,1), include the H-mode data from small tokamaks and predict ~20% higher confinement for an ITER-like machine than the three others, IPB98(y,2), IPB98(y,3), and IPB98(y,4), which exclude these data. In the IPB, it is concluded that the available physical and empirical evidence is not strong enough to justify a preferential recommendation among these log-linear scalings. IPB98(y,2) has therefore been selected as a conservative option. Thermal energy confinement in the ELMy H-mode described by the IPB98(y,2) scaling is

$$\tau_{E,th}^{IPB98(y,2)} = 0.0562 I_p^{0.93} B_T^{0.15} P^{-0.69} n_e^{0.41} M^{0.19}$$
$$\times R^{1.97} \epsilon^{0.58} \kappa_x^{0.78}$$

(in s, MA, T, MW, 10^{19} m^{-3}, AMU, and m)

(rms error 0.145) ,

where the elongation κ_a is defined as $\kappa_a = S_o/(\pi a^2)$ with S_o the plasma cross-sectional area. The 2σ log-linear or the 1σ log nonlinear interval for this scaling is approximately $\pm 20\%$. Adoption of this scaling does not generally change the conclusions and tendencies of the parameter survey described in Secs. IV and V.

TABLE V

Parameters of ITER-FEAT Inductive Operation Scenario

Parameter	500 MW	Parameter	500 MW
R/a (m/m)	6.2/2.0	$P_{RF} + P_{NB}$ (MW)	17 + 33
Volume (m^3)	831	P_{OH} (MW)	1
Surface (m^2)	683	P_{TOT} (MW)	151
Separator length (m)	18.2	P_{BRM} (MW)	26
$S_{cross\ section}$ (m^2)	21.9	P_{SYN} (MW)	8
B_T (T)	5.3	P_{LINE} (MW)	27
I_P (MA)	15.0	P_{RAD} (MW)	61
κ_a/δ_a	1.85/0.48	P_{fus} (MW)	500
κ_{95}/δ_{95}	1.70/0.33	P_{LOSS}/P_{LH}	104/51
l_i (3)	0.84	Q	10
V_{LOOP} (mV)	75	τ_E (s)	3.4
q_{95}	3	W_{th} (MJ)	353
β_N	2.0	W_{fast} (MJ)	34
n_e (10^{19} m^{-3})	11.3	$H_{H(y,2)}$	1.0
n_e/n_{GW}	0.94	τ_{He}^*/τ_E	5
$\langle T_e \rangle$ (keV)	8.9	$Z_{eff,\ ave}$	1.72
$\langle T_i \rangle$ (keV)	8.1	$f_{He,axis/ave}$ (%)	4.4/3.2
$\langle \beta_T \rangle$ (%)	2.8	$f_{Be,axis}$ (%)	2.0
β_p	0.72	$f_{Ar,axis}$ (%)	0.14

The main plasma parameters of ITER-FEAT in the reference inductive operation are shown in Table V. Compared with IAM, the plasma current was increased in ITER-FEAT to compensate for the penalty imposed by the choice of conservative energy confinement scaling. Increase of the plasma current was realized by slightly decreasing the aspect ratio or by increasing the plasma minor radius from 1.9 to 2.0 m with the same major radius. Other parameters are basically the same.

Operation regimes of ITER-FEAT based on zero-dimensional modeling are shown in Figs. 13 through 16.
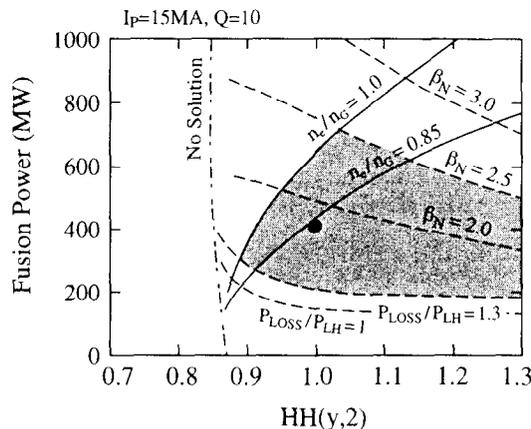

Fig. 14. The $Q = 10$ operation domain (zero-dimensional modeling) with $I_p = 17$ MA ($\tau_{He}^*/\tau_E = 5$, Be = 2%, Ar = 0.12%).
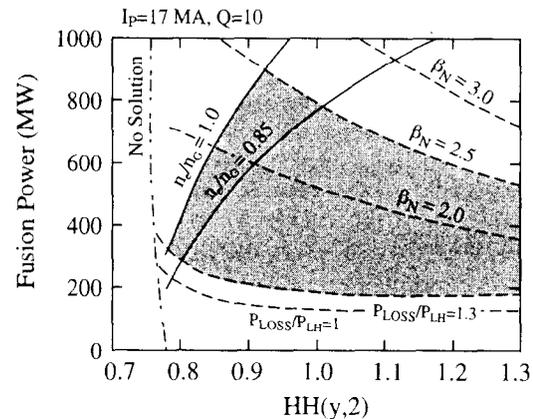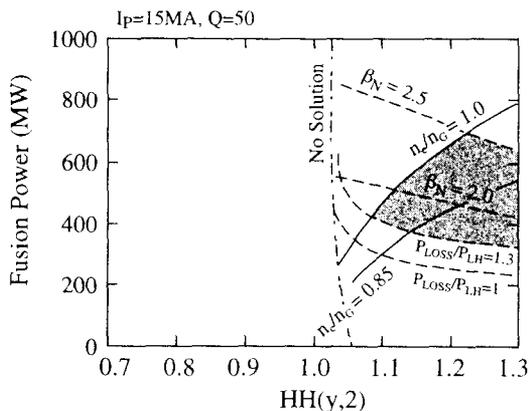

Fig. 13. The $Q = 10$ operation domain (zero-dimensional modeling) with $I_p = 15$ MA ($\tau_{He}^*/\tau_E = 5$, Be = 2%, Ar = 0.12%).

Figure 13 shows the $Q = 10$ operational domain of ITER-FEAT. As a consequence of adopting new scaling for the H-mode transition power, the lower boundary of the operation regime was extended to the smaller fusion power side compared with the operation domain of IAM computed with optimistic confinement scaling. The confinement margin, operation below $H_H = 0.9$, is very small with ITER-FEAT because of adoption of the more conservative energy confinement scaling than before. On the other hand, the upper limit set by the β_N has become

Fig. 15. The $Q = 50$ operation domain (zero-dimensional modeling) with $I_p = 15$ MA $(\tau^*_{He}/\tau_E = 5, Be = 2\%, Ar = 0.12\%)$.
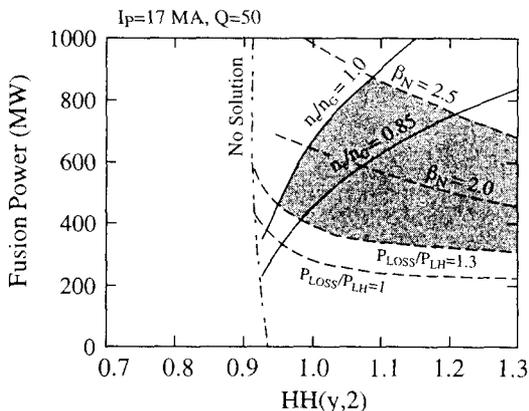

Fig. 16. The $Q = 50$ operation domain (zero-dimensional modeling) with $I_p = 17$ MA $(\tau^*_{He}/\tau_E = 5, Be = 2\%, Ar = 0.12\%)$.

less stringent. The present reference design of ITER does not fully support a 400-s burning discharge at 17 MA. However, 17-MA operation would be possible if the flattop discharge length is limited to 100 s. Figure 14 shows that the $Q = 10$ operation domain will be very much expanded when the plasma current is increased to 17 MA.

The requirement for the RC/RTO ITER still asks to maintain the possibility of ignition. Figure 15 shows that if sufficiently good confinement $(H_H > 1.1)$ is achieved, high-Q operation, $Q > 50$ should be possible. Figure 16 shows that if the plasma current can be increased to 17 MA, there is a possibility of very high Q operation even with $H_H = 1.0$.

VII. SUMMARY

Machine parameters and configurations of the ITER-FEAT were determined through system code analysis to achieve the revised technical goals of ITER under the constraints of the engineering limits and minimum cost target. A conservative physics assumption on energy confinement scaling was adopted, and it has been shown that the technical goals of ITER are achievable with the recently selected machine parameters of ITER-FEAT.

ACKNOWLEDGMENTS

REFERENCES

1. "Technical Basis for the ITER Final Design Report, Cost Review and Safety Analysis," ITER EDA Documentation Series No.16, International Atomic Energy Agency (1998).

2. "ITER Council Proceedings: 1999," ITER EDA Documentation Series No. 17, International Atomic Energy Agency (1999).

3. D. BOUCHER et al., in *Proc. 16th Fusion Energy Conf.*, Montreal, Canada, 1996, p. 945, International Atomic Energy Agency (1997).

4. "ITER Physics Basis," *Nucl. Fusion*, **39**, *12* (1999).

5. F. LEVINTON et al., "Improved Confinement with Reversed Magnetic Shear in TFTR," *Phys. Rev. Lett.*, **75**, 4417 (1995).

6. E. STRAIT et al., "Enhanced Confinement and Stability in DIII-D Discharges with Reversed Magnetic Shear," *Phys. Rev. Lett.*, **75**, 4421 (1995).

7. JET TEAM, "Optimization of JET Plasmas with Current Profile Control," *Proc. 16th Int. Conf. Fusion Energy*, Montreal, Canada, 1996, Vol. 1, p. 487, International Atomic Energy Agency (1997).

8. H. SHIRAI and JT-60 TEAM, "Recent Progress in JT-60U Experiments with W-Shaped Divertor Configuration," presented at 39th Annual Mtg. American Physical Society Division of Plasma Physics, Pittsburgh, Pennsylvania, 1997.

9. D. PFIRSCH and H. TASSO, "A Theorem on MHD-Instability of Plasmas with Resistive Walls," *Nucl. Fusion*, **11**, 259 (1971).

10. E. J. STRAIT, "Stability of High Beta Tokamak Plasmas," *Phys. Plasmas*, **1**, 1415 (1994).

Hiroshi Matsumoto (PhD, University of Tokyo, Japan, 1985) has been working with the Joint Central Team of ITER since 1992 in the areas of design integration and physics. His background is as an experimental physicist working on the JFT-2M at the Japan Atomic Energy Research Institute and DIII-D in General Atomics (GA). His current interest is development of operation and control scenarios for ITER.

Pietro Barabaschi (ME, University of Genoa, Italy, 1989) heads the Design Integration Unit of the ITER Joint Central Team at the Garching Joint Work Site. His work covers broad and important areas of tokamak design, such as structural analysis, electromagnetic analysis, system analysis, and design integration.

Yoshiki Murakami (Dr Eng, University of Tokyo, Japan, 1989) is a visiting researcher with the Joint Central Team of ITER. His current work is in the area of core plasma transport analysis and development of operation scenarios for ITER. His interests include plasma edge physics and divertor simulation. He is on loan from Power and Industrial Systems R&D Center, Toshiba Corporation, Japan.